Generalized gradient approximation calculations of the pressure-induced phase transition of $YAlO_3$ perovskite

2006 J. Phys.: Condens. Matter 18 3907

(http://iopscience.iop.org/0953-8984/18/16/001)

INSTITUTE OF PHYSICS PUBLISHING JOURNAL OF PHYSICS: CONDENSED MATTER

J. Phys.: Condens. Matter **18** (2006) 3907–3916 doi:10.1088/0953-8984/18/16/001

Generalized gradient approximation calculations of the pressure-induced phase transition of $YAlO_3$ perovskite

Xiang Wu[1], **Shan Qin**[2] **and Ziyu Wu**[1,3]

[1] Beijing Synchrotron Radiation Facility, Institute of High Energy Physics, Chinese Academy of Sciences, Beijing 100049, People's Republic of China
[2] Department of Geology, Peking University, Beijing 100871, People's Republic of China

E-mail: wuzy@ihep.ac.cn

Received 6 December 2005, in final form 14 February 2006
Published 3 April 2006
Online at stacks.iop.org/JPhysCM/18/3907

Abstract

An investigation into the high-pressure behaviour of $YAlO_3$ perovskite was conducted using first-principles calculations based on density functional theory within the generalized gradient approximation. Five candidate phases were considered, $Pbnm$, $Cmcm$, $I4/mcm$, $P4/mbm$ and $Pm3m$ respectively. Our results demonstrate a phase transition of $YAlO_3$ from $Pbnm$ to $I4/mcm$ at 80 GPa and 0 K, and no tendency to the cubic phase or the post-perovskite phase in our pressure range. This high-pressure behaviour of $YAlO_3$ is similar to that of $CaSiO_3$. The pressure dependence of the distortion of AlO_6 octahedra is described by the octahedral tilting and rotation angles, the tolerance factor, the polyhedral volume ratio and the valence charge density. We also summarize the relations between tolerance factor, bulk modulus and radius of the A-site in $Pbnm$-$AAlO_3$ systems.

(Some figures in this article are in colour only in the electronic version)

1. Introduction

Oxide perovskites with the general formula ABO_3 are of great interest in materials science due to diverse physical properties [1], and in Earth sciences due to perovskite-type (pv) $(Mg, Fe)SiO_3$, believed to the most abundant mineral in the Earth's lower mantle [2]. The ideal perovskite structure has $Pm3m$ symmetry with the A cation in the centre of a cube defined by eight corner-sharing BO_6 octahedra. However, most perovskites are derived from the ideal via the titling and distortion of the BO_6 octahedra, and they are of lower symmetries such as tetragonal and orthorhombic. The effect of increasing pressure or/and temperature on the tilting of the octahedra might lead to phase transformations between orthorhombic,

[3] Author to whom any correspondence should be addressed.

rhombohedral, tetragonal and cubic symmetries, such as the sequence of phase transition ($Pbnm$–$I4/mcm$–$Pm3m$) in $SrZrO_3$ [3] and $CaTiO_3$ [4, 5] at elevated temperatures, and the structural distortion of $CaTiO_3$ under compression [6, 7]. Since the discovery of $MgSiO_3$ post-perovskite (ppv) phase with the $CaIrO_3$ structure ($Cmcm$) under conditions approaching those of the lowermost mantle [8–10], which could explain some of the observed phenomena in the D'' layer, interest in the pressure-induced phase transitions of perovskites has become more popular [7, 11–15].

Published data show that the most important components of the Earth's lower mantle, $MgSiO_3$ and $CaSiO_3$, show different behaviour of structural phase transitions under compressions, i.e. $MgSiO_3$ undergoes a pv-to-ppv phase transition [8–10], whereas $CaSiO_3$ transits into a tetragonal phase [16]. As a structural analogue, the orthorhombic $YAlO_3$ ($Pbnm$) has been investigated with respect to the high-pressure behaviour by Ross *et al* [17, 18], although with both cations having a formal charge of +3 it is different from $MgSiO_3$ and $CaSiO_3$. The first study up to 4 GPa suggested that AlO_6 octahedra are more compressible than the YO_{12} site and that the Al–O–Al octahedral tilting decreases with pressure [17]. The second study up to 8.5 GPa with high precise resolution verified that the structure of $YAlO_3$ perovskite becomes less distorted with increasing pressure [18]. The same behaviour is also observed in $GdAlO_3$ perovskite, and it was further predicted that a possible transition occurs at 12 GPa from orthorhombic to tetragonal symmetry [19]. The orthorhombic perovskites $LaFeO_3$ and $PrFeO_3$ are both also reported that they undergo a first-order phase transition to a new high-pressure phase, a proposed tetragonal structure [20]. Recently, Zhao *et al* used the bond valence concept to develop a model (the relative compressibilities of the octahedral and dodecahedral cations sites in the perovskite structure) that predicts the structural behaviour of the oxide perovskites at high pressure [21]. According to this model, most perovskites with $A^{3+}B^{3+}O_3$ become less tilted and the structures evolve towards a higher-symmetry configuration. However, an *ab initio* study of $ScAlO_3$ showed that the $Pbnm$ phase is stable relative to the cubic structure up to pressures of ∼200 GPa and temperatures of ∼800 K [22]. Until now, few high-pressure phases (space group) have been determined and characterized for $A^{3+}B^{3+}O_3$ perovskites. Available data show that there are several candidate high-pressure phases for the $Pbnm$-perovskites: $I4/mcm$ observed in $CaSiO_3$ [16], $P4/mbm$ and $Pm3m$ predicted by group–subgroup relationships [23, 24], and post-perovskite $Cmcm$ found to be stable for $MgSiO_3$ [8–10].

In this paper, therefore, we will select $YAlO_3$ as our object, and consider all the different phases, either those experimentally detected or those proposed by analogy with other compounds, with an aim to fully characterize ambient and high-pressure phases of $YAlO_3$. We will present a fully *ab initio* calculation method based on density functional theory (DFT), which is a very accurate method for solving the total energy problem and which has been proven to be successful in studying phase transitions in our previous work [7, 25, 26]. We will compute the equation of state for each phase, as well as the transition pressures between them, provide insight into the atomistic controls on the structural changes, and further discuss and summarize the high-pressure behaviours of $A^{3+}AlO_3$ perovskites. The rest of this paper is organized as follows: the calculation methods and the system are described in section 2; results and discussion of the structural stabilities under high pressures are presented in section 3; finally a brief conclusion is given in section 4.

2. Calculation method

Five candidate phases of $YAlO_3$ were designed: $Pbnm$, $Cmcm$, $P4/mbm$, $I4/mcm$ and $Pm3m$ respectively. We used the experimental unit cell parameters or those of analogue

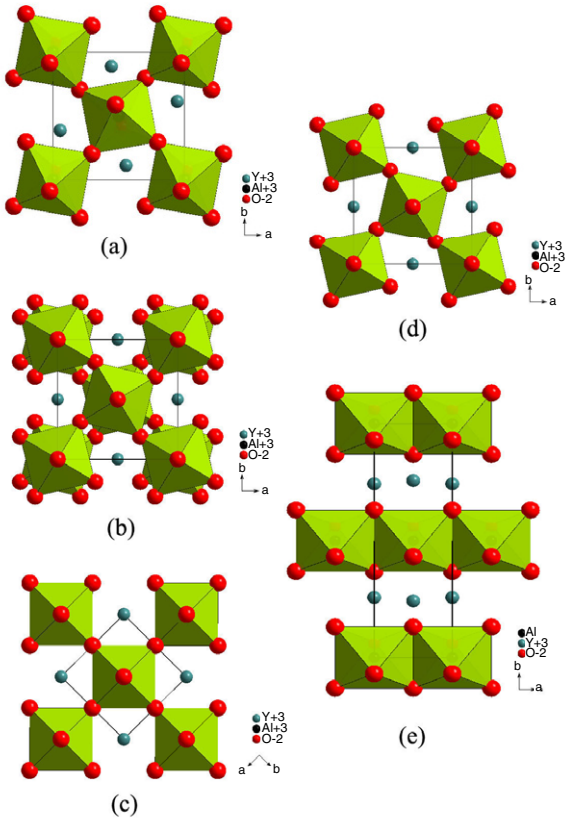

Figure 1. The phases of $YAlO_3$ studied here: $Pbnm$ (a), $I4/mcm$ (b), $Pm3m$ (c), $P4/mbm$ (d), and $Cmcm$ (e). The octahedra consist of oxygen and aluminium.

materials as the initial models for the above phases. Figure 1 represents the schematic crystal structures of candidate phases of $YAlO_3$.

The first-principles calculations performed in this paper are based on density functional theory (DFT). The total energies have been calculated within the full potential augmented plane wave (FPAPW) + local orbitals (lo) method, implemented in WIEN2K code [27]. The effects of the approximation to the exchange-correlation energy were treated by the generalized gradient approximation (GGA) [28]. In order to increase the reliability and make a reasonable comparison, we used the same radius of the muffin-tin sphere for the same kind of atom in all calculations. The muffin-tin radii of Y, Al and O were chosen to be 1.6, 1.5 and 1.7 au respectively. In the APW calculations, we set the energy threshold between core and valence states at -8.0 Ryd. For the number of plane waves, the criterion used was muffin-tin radius multiplied by $K_{\max}$ (for the plane waves), yielding a value of 7.0. 500 k-points were specified in the whole Brillouin zone (BZ). For each crystalline phase, we calculated the minimum total energy of the unit cell for a number of different volumes. We did not perform the structure optimization of the $Pm3m$ phase, but just specified the convergence criterion (the different charge <0.0001) in the self-consistency cycle. In other phases, we optimized the lattice parameter ratios (b/a and/or c/a) for each volume and relaxed all independent internal atomic coordinates until the forces on every atom were below a tolerance value taken as 1 mRyd/bohr.

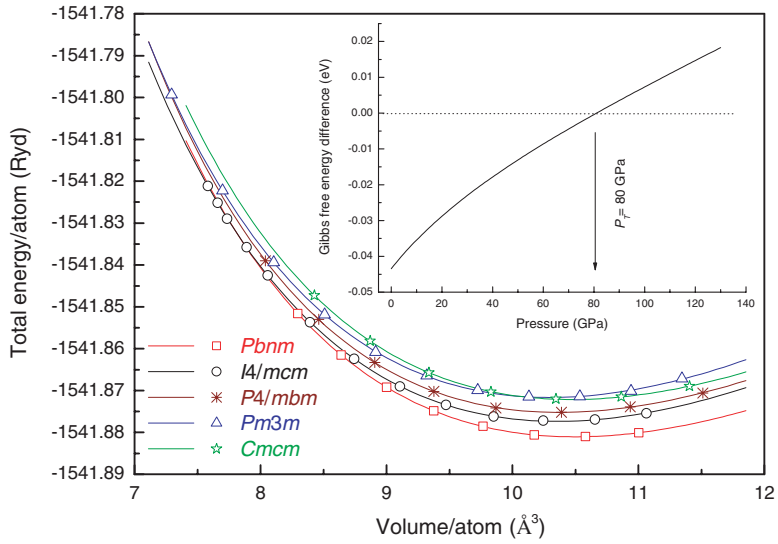

Figure 2. Calculation of the total energy versus volume for five candidate phases of $YAlO_3$. The inset: calculated Gibbs free energy differences versus pressure for both $Pbnm$ and $I4/mcm$ phases.

Once the minimum total energies of every phase are obtained at different volumes, they are fitted to the Murnaghan equation of state [29], as below:

$$E(V) = E_0 - \frac{B_0 V_0}{B_0' - 1} + \frac{B_0 V}{B_0'}\left[\frac{(V_0/V)^{B_0'}}{B_0' - 1} + 1\right] \tag{1}$$

where B_0 and B_0' are the bulk modulus and its derivative respectively, E_0 is the ground-state total energy and V_0 is the equilibrium volume. On the other hand, the relevant thermodynamic potential is the Gibbs free energy G, and the stable structure is the one with the lowest G. In this study the temperature is limited to $T = 0$ K, so G is equal to the enthalpy H, as follows:

$$G(P) = E_0 + \frac{B_0 V_0}{B_0' - 1}\left[\left(1 + \frac{B_0'}{B_0}P\right)^{\frac{B_0' - 1}{B_0'}} - 1\right]. \tag{2}$$

If a transition between two phases occurs, in both phases G will be equal at the transition pressure P_T. Alternatively, the transition pressure may be obtained as the negative slope of the common tangent between the two $E_{tot}(V)$ curves.

3. Results and discussion

We optimized the structures and obtained the ground-state lowest total energies. Figure 2 shows the total energy versus volume curves for the five phases of $YAlO_3$. The solid lines are the fit of the computed data using the Murnaghan equation of state (equation (1)). The theoretical ground-state parameters obtained are listed in table 1, which also includes the available experimental data for comparison. It is clear that the theoretical values agree very well with the experimental values; for example, the estimated errors are within 3% for the equilibrium volumes, which is typical for *ab initio* DFT methods.

As is seen in figure 2, the lowest energies (empty squares) correspond to the $Pbnm$ phase, it being the most stable structure at ambient conditions. When the average volume per atom

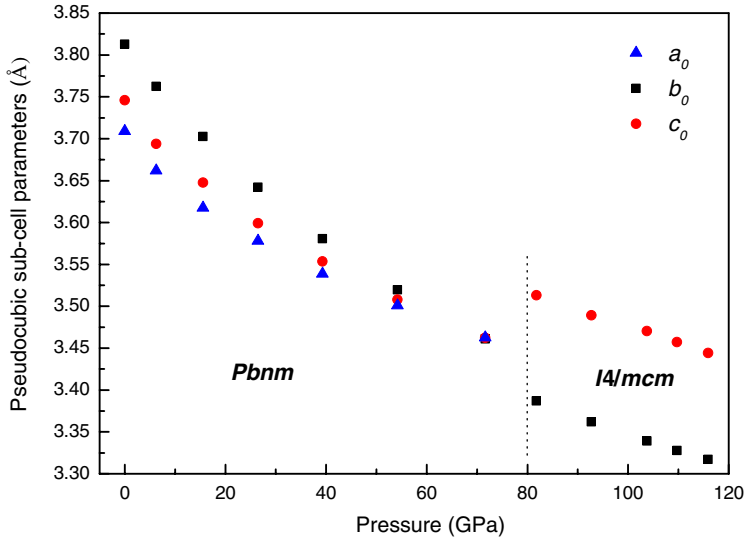

Figure 3. Pseudocubic sub-cell parameters plotted as a function of pressure in the $YAlO_3$ system. $a_0 = a/\sqrt{2}$, $b_0 = b/\sqrt{2}$, $c_0 = c/2$, where a, b, and c are the lattice parameters of the unit cell.

Table 1. The equilibrium volume per primitive cell, the bulk modulus and its derivative for five candidate phases of $YAlO_3$.

$YAlO_3$	V_0 (Å^3)	B_0 (GPa)	B_0'
Pbnm	52.475	188	3.82
Experimental [18]	50.851	192	7.3
Cmcm	52.325	190	3.85
*P*4/*mbm*	51.85	194	3.95
*I*4/*mcm*	51.75	199	3.68
*Pm*3*m*	51.47	206	3.65

is smaller than 8 Å^3, the E–V cures of *Pbnm* and *I*4/*mcm* phases nearly superpose, which indicates that a phase transition occurs from *Pbnm* to *I*4/*mcm*. According to the ΔG–P curves (the inset of figure 2), the phase transition pressure is 80 GPa. At this critical pressure, the volume collapse is only 0.62%. The above information indicates that the *Pbnm*-to-*I*4/*mcm* transition is of near second order, whereas the discontinuous lattice constants are observed evidently in figure 3. In addition, *Pbnm* is not a subgroup of *I*4/*mcm* [23, 24], which also means that the *Pbnm*-to-*I*4/*mcm* phase transition is required to be first order, based on symmetry considerations. This transition has been confirmed to be first order in the $SrRuO_3$ case [30]. In a word, *Pbnm*-$YAlO_3$ undergoes a first-order transition to the *I*4/*mcm* phase at high pressure. However, the other phases (*P*4/*mbm*, *Pm*3*m* and *Cmcm*) are unstable in the present pressure range at 0 K; for example, the Gibbs free energies of *Pm*3*m* are still higher than those of *I*4/*mcm* up to 142 GPa.

Previous studies have shown that the distortion degree of perovskite is often described by the following parameters: the BO_6 octahedral tilting and rotation [31, 32], the tolerance factor (t) [33], and the polyhedral volume ratio V_A/V_B, where V_A is the volume of the A-site polyhedron and V_B is that of the B-site polyhedron [34–36]. The tilting angle (∠B–O1–B) and the rotation angle (∠B–O2–B) of the octahedron, t and V_A/V_B for the ideal perovskite are

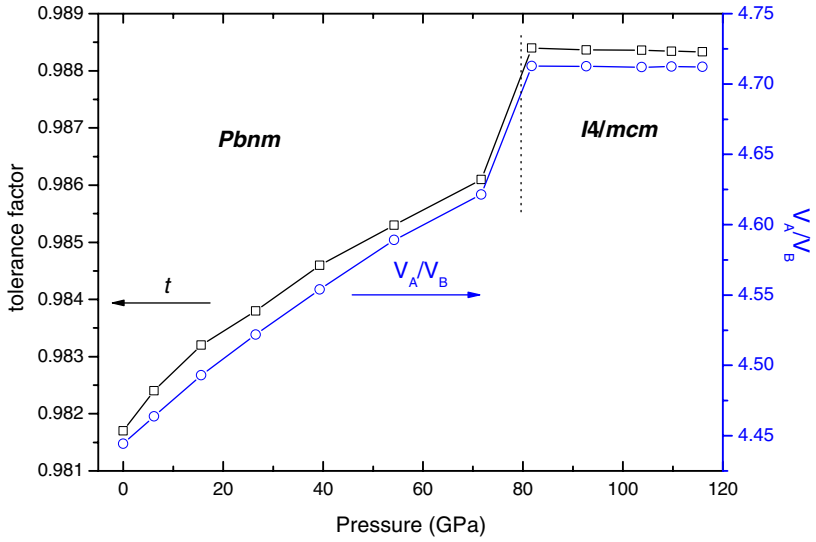

Figure 4. Plot of t and V_A/V_B of $YAlO_3$ versus pressure. The value of V_A/V_B is calculated using the software IVTON [37]. $t = \overline{Y-O}/(\sqrt{2} * \overline{Al-O})$, $\overline{Y-O}$ is the mean value of twelve Y–O bond distances and $\overline{Al-O}$ is that of six Al–O bond distances.

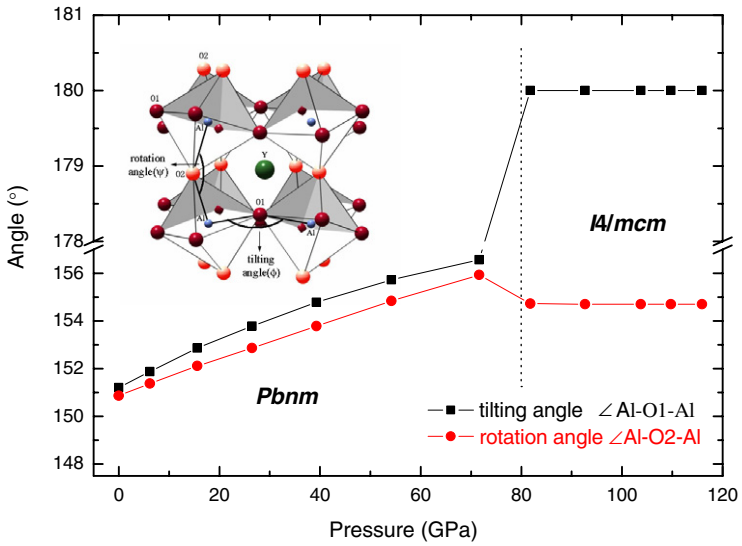

Figure 5. The tilting angle and the rotation angle of AlO_6 octahedra versus pressure. The bond angle ∠Al–O1–Al is the tilting angle of the octahedron relative to the (001) plane and the ∠Al–O2–Al is the rotation angle around the c axis. They are represented by the inset figure.

180°, 180°, 1 and 5 respectively. According to the optimized atomic coordinates, we calculated the above parameters of both $Pbnm$ and $I4/mcm$ at diverse pressures. Figures 4 and 5 show that the four parameters of $Pbnm$-$YAlO_3$ increase with the applied pressure, towards the ideal values, indicating that pressure decreases the $YAlO_3$ structural distortion, which is consistent with the experimental results [17, 18] and the theoretical model prediction [21]. At the phase transition pressure, there are abrupt increases for the parameters except the ∠Al–O2–Al. In

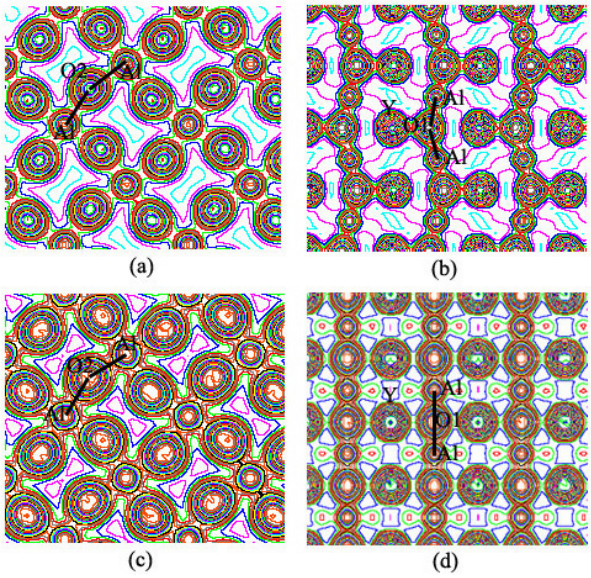

Figure 6. The valence charge density in the specified plane. (a) The (001) plane including the ∠Al–O2–Al, and (b) the (010) plane including the ∠Al–O1–Al, of the $Pbnm$ phase at 6.2 GPa; (c) and (d) are those of the $I4/mcm$ phase correspondingly at 116.0 GPa.

particular, ∠Al–O1–Al becomes 180° suddenly, which leads to a sudden increase in the c-axis lattice constant in the $I4/mcm$ phase (figure 3). The valence charge density clearly shows the changes of both ∠Al–O1–Al and ∠Al–O2–Al in the $Pbnm$ and $I4/mcm$ phases, as represented in figure 6. Comparing figures 6(b) and (d), we found that the Y and O1 ions are in special positions in the high-pressure phase, in contrast to being in general positions in the low-pressure phase. However, t, V_A/V_B and ∠Al–O2–Al of $I4/mcm$-$YAlO_3$ show a very slight decrease with increasing pressures from 82 to 116 GPa, and the c/a ratio rises slightly with pressure, which indicates that pressure enhances the $I4/mcm$-$YAlO_3$ structural distortion. This is consistent with a phase transformation from $I4/mcm$ to $Pm3m$ not occurring under high pressure at 0 K. Despite the increasing distortion of the $I4/mcm$ phase, there is no tendency to evolve to the $Cmcm$ (ppv) phase with more distortion. The energy difference between $I4/mcm$ and $Cmcm$ (figure 2) is large enough to say that this phase does not yet occur. The same behaviour is also observed in $I4/mcm$-$CaSiO_3$ under compression [16].

$AAlO_3$ (A = Sc, Y, Sm, Gd, Tb and Ho) all have the $Pbnm$ structure at ambient conditions. Both experimental and theoretical calculation results indicate the distortion of orthorhombic $YAlO_3$ and $GdAlO_3$ decreasing with pressure. However, the distortion of $Pbnm$-$ScAlO_3$ shows no significant change with increasing pressure [38]. The reason is that the experimental pressure is too low to distinguish the slight change, only 5 GPa. *Ab initio* calculations show that the $Pbnm$-$ScAlO_3$ does not transit into the $Pm3m$ phase up to 200 GPa, like the behaviour of $YAlO_3$ in our calculations, but pressure dependence of the distortion was not analysed and the tetragonal phases were not considered in their work [22]. According to the model prediction of Zhao *et al* [21], the distortion of $Pbnm$-$ScAlO_3$ also decreases with increasing pressure. Figure 7 illustrates the linear increase relation between the tolerance factor and the radius of A^{3+} (VIII), which indicates that the distortion of $Pbnm$-$AAlO_3$ decreases with increasing the radius of the A-site. Connecting with the above discussion, thus, we can conclude that it is more difficult to evolve towards a higher-symmetry configuration under compression for $AAlO_3$ with

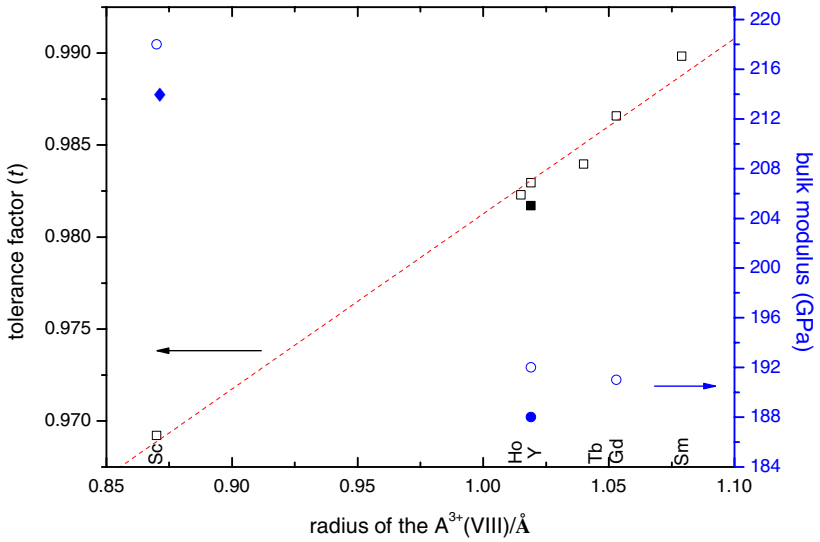

Figure 7. The relations between tolerance factor, bulk modulus and radius of the A-site in *Pbnm*-$AAlO_3$ systems. The calculation method for the tolerance factor is the same as in figure 4. Solid square and circle: our calculations; solid diamond: theoretical result of [22]; open square and circle: experimental data for $ScAlO_3$ [38], $YAlO_3$ [18], $GdAlO_3$ [19], $HoAlO_3$ (ICSD-39606), $TbAlO_3$ (ICSD-84422), and $SmAlO_3$ (ICSD-10334). The radii of A^{3+} (VIII) are from [39]. The dashed line is the least-squares fit of the tolerance factors using a linear A^{3+} (VIII)-dependent function.

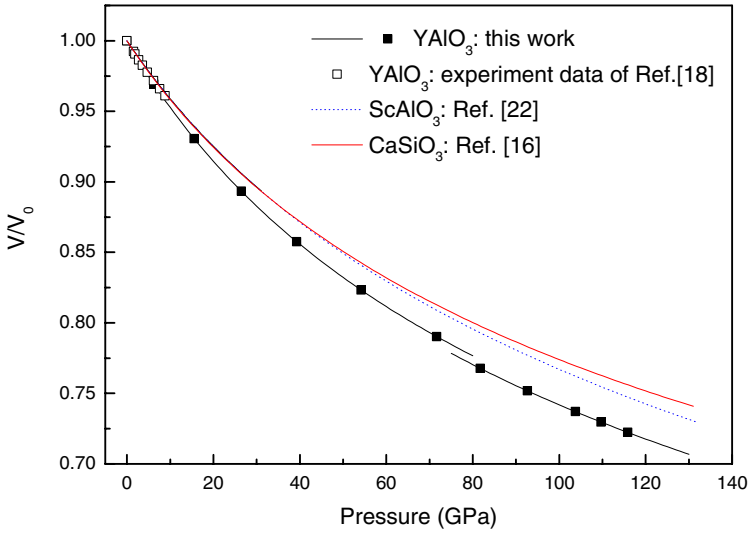

Figure 8. Comparison of pressure against the V/V_0 for $ScAlO_3$, $YAlO_3$ and $CaSiO_3$.

smaller radius of the A-site; for example, the phase transition pressure for $YAlO_3$ is 80 GPa, larger than that for $GdAlO_3$ (an extrapolated value of 12 GPa). In figure 8, we also display the available values of bulk moduli of *Pbnm*-$AAlO_3$ versus the trivalent cation radius. Due to the limited available data, a quantitative relation is not obtained, but the qualitative trend is that the bulk modulus is smaller with the cation radii being bigger.

Because of their being structural analogues and having similar high-pressure behaviour, it is interesting for orthorhombic $ScAlO_3$ and $YAlO_3$ to be compared with orthorhombic $CaSiO_3$ perovskite. The pressure–volume equation of state of these three perovskites is plotted in figure 7. Our results (solid squares and black solid line) are in excellent agreement with the experimental data for $YAlO_3$, as presented by the empty squares. The curves for both $Pbnm$ and $I4/mcm$ of $CaSiO_3$ are continuous; there is no volume collapse at the critical pressure (14.2 GPa). The closeness between the $ScAlO_3$ curve and the $CaSiO_3$ curve indicates that the properties of $ScAlO_3$ can reasonably approximate those of $CaSiO_3$. Theoretical calculations have predicted that $YAlO_3$ and $CaSiO_3$ undergo a pressure-induced phase transition from $Pbnm$ to $I4/mcm$, thus we boldly predict that $ScAlO_3$ has the same behaviour under compression.

4. Conclusion

In conclusion, *ab initio* calculations based on DFT within the GGA present a phase transition of $YAlO_3$ from $Pbnm$ to $I4/mcm$ at 80 GPa and 0 K, and no tendency to the cubic phase or the post-perovskite phase in our pressure range. The pressure dependence of the distortion of AlO_6 octahedra was described in detail by the octahedral tilting and rotation angles, the tolerance factor, the polyhedral volume ratio and the valence charge density, which is that pressure decreases the $Pbnm$-$YAlO_3$ structural distortion, in contrast to enhancing that of $I4/mcm$ slightly. We summarize the relations between tolerance factor, bulk modulus and radius of A-site in $Pbnm$-$AAlO_3$ systems, which are that the t versus radii shows a quasi-linear increase, and the bulk modulus is smaller with the cation radii being bigger. The high-pressure behaviour of $YAlO_3$ is similar to that of $CaSiO_3$. We also predict that $ScAlO_3$ has the same behaviour and that its properties can approximate those of $CaSiO_3$.

Acknowledgments

Z Y Wu acknowledges the financial support of the Outstanding Youth Fund (10125523), the Key Important Nano-Research Project (90206032) of the National Natural Science Foundation of China, and also the Pilot Project of the Knowledge Innovation Program of the Chinese Academy of Sciences (KJCX2-SW-N11). S Qin thanks the National Natural Sciences Foundation of China for financial support (40272023).

References

[1] Lufaso M W and Woodward P M 2001 *Acta Crystallogr.* B **57** 725
[2] Knittle E and Jeanloz R 1987 *Science* **235** 668
[3] Kennedy B J, Howard C J and Chakoumakos B C 1999 *Phys. Rev.* B **59** 4023
[4] Redfern S A T 1996 *J. Phys.: Condens. Matter* **8** 8267
[5] Kennedy B J, Howard C J and Chakoumakos B C 1999 *J. Phys.: Condens. Matter* **11** 1479
[6] Wu X, Qin S, Wu Z Y, Dong Y H, Liu J and Li X D 2004 *Acta Phys. Sin.* **53** 1967
[7] Wu X, Dong Y H, Qin S, Abbas M I and Wu Z Y 2005 *Solid State Commun.* **136** 416
[8] Murakami M, Hirose K, Kawamura K, Sata N and Ohishi Y 2004 *Science* **304** 855
[9] Iitaka T, Hirose K, Kawamura K and Murakami M 2004 *Nature* **430** 442
[10] Oganov A R and Ono S 2004 *Nature* **430** 445
[11] Hirose K, Kawamura K, Ohishi Y, Tateno S and Sata N 2005 *Am. Mineral.* **90** 262
[12] Liu H Z, Chen J, Hu J, Martin C D, Weidner D J, Häusermann D and Mao H K 2005 *Geophys. Res. Lett.* **32** L04304
[13] Mao W L, Shen G, Prakapenka V B, Meng Y, Campbell A J, Heinz D L, Shu J, Hemley R J and Mao H K 2004 *Proc. Natl Acad. Sci. USA* **101** 15867

[14] Oganov A R and Price G D 2005 *J. Chem. Phys.* **122** 124501
[15] Belonoshko A B, Skorodumova N V, Rosengren A, Ahuja R, Johansson B, Burakovsky L and Preston D L 2005 *Phys. Rev. Lett.* **94** 195701
[16] Jung D Y and Oganov A R 2005 *Phys. Chem. Minerals* **32** 146
[17] Ross N L 1996 *Phase Transit.* **58** 27
[18] Ross N L, Zhao J and Angel R J 2004 *J. Solid State Chem.* **177** 1276
[19] Ross N L, Zhao J, Burt J B and Chaplin T D 2004 *J. Phys.: Condens. Matter* **16** 5721
[20] Xu W M, Naaman O, Rozenberg G Kh, Pasternak M P and Taylor R D 2001 *Phys. Rev.* B **64** 094411
[21] Zhao J, Ross N L and Angel R J 2004 *Acta Crystallogr.* B **60** 263
[22] Magyari-Köpe B, Vitos L and Kollár J 2001 *Phys. Rev.* B **63** 104111
[23] Aleksandrov K S 1976 *Ferroelectrics* **14** 801
[24] Howard C J and Stokes H T 1998 *Acta Crystallogr.* B **54** 782
[25] Wu X, Qin S and Wu Z Y 2005 First-principles study of structural stabilities, electronic and optical properties of CaF_2 under high pressure *Phys. Rev.* B at press
[26] Wu X and Wu Z Y 2005 Theoretical calculations of the high-pressure phases of ZnF_2 and CdF_2 *Eur. Phys. J.* B at press
[27] Blaha P and Schwarz K 2002 *WIEN2k* Vienna University of Technology Austria
[28] Perdew J P, Burke K and Ernzerhof M 1996 *Phys. Rev. Lett.* **77** 3865
[29] Murnaghan F D 1944 *Proc. Natl Acad. Sci. USA* **50** 667
[30] Kennedy B J and Hunter B A 1998 *Phys. Rev.* B **58** 653
[31] Glazer A M 1972 *Acta Crystallogr.* B **28** 3384
[32] Glazer A M 1975 *Acta Crystallogr.* A **31** 756
[33] Goldschmidt V M 1926 *Skr. Nor. Vidensk.-Akad. Oslo, I: Mat.-Natur. K1* 2
[34] Thomas N W 1996 *Acta Crystallogr.* B **52** 16
[35] Thomas N W 1998 *Acta Crystallogr.* B **54** 585
[36] Magyari-Köpe B, Vitos L, Johansson B and Kollár J 2001 *Acta Crystallogr.* B **57** 491
[37] Zunic T B and Vickovic I 1996 *J. Appl. Crystallogr.* **29** 305
[38] Ross N L 1998 *Phys. Chem. Minerals* **25** 597
[39] Shannon R D 1976 *Acta Crystallogr.* A **32** 751